5 Nanowires for Metal-Ion Batteries

Santosh J. Uke[1] *and Satish P. Mardikar*[2]
[1]Department of Physics, JDPS College, Sant Gadge Baba Amravati University, Amravati, India
[2]Department of Chemistry, SRS College, Sant Gadge Baba Amravati University, Amravati, India

CONTENTS

5.1 INTRODUCTION

With the ever-increasing demand for electrical energy, the development of metal-ion batteries with high volumetric capacity, high gravimetric capacity, high energy density, high power density, long cycling life, safe and low cost gained enormous attention. Metal-ion batteries have a key role in renewable energy systems. Over the years, lithium-ion batteries (LIBs) have been the common source of electrical energy for portable electronics like mobile phones and laptops. Also, it fulfills the energy needs of electric and hybrid vehicles. Interestingly, recently due to the limited resources of lithium metal in the Earth's crust and its high cost, the different metal-ion batteries viz. the sodium-ion battery, magnesium-ion battery, aluminum-ion battery, etc., have gained enormous attention as a secondary energy source to fulfill the need as a power back system and alternative power source in the global energy market. The Na-, Mg-, and Al-ion batteries are the most promising and low-cost alternative solutions for global energy needs [1,2]

Na is the fourth most abundant element on the Earth, second to that Al and Mg metal are also abundant in nature. Recently, due to the similarity in energy storage mechanism and low cost, batteries based on Na-, Mg-, and Al- metals are highly studied. The metal-ion (Na, Mg, and Al) batteries show a higher specific and volumetric capacity than LIBs. Moreover, in addition to the advantages associated with metal-ion batteries, there are different issues related to these batteries [3,4]. The different components of batteries such as substrate, electrode, electrolyte, separator, etc. have their special importance in the demonstration of high volumetric capacity, high gravimetric capacity, high energy density, high power density, and long cycle life at the external load. Recently, to enhance the performance of metal-ion batteries in the form of energy density, power density, and

DOI: 10.1201/9781003296621-5

cycle life, many research communities have adopted many advanced strategies. This includes synthesis of new electrode and electrolyte materials, modification in electrode fabrication techniques, advancement in complete cell fabrication, use of solid electrolytes, etc.

The energy stored in metal-ion batteries solely depends on the active material used for the fabrication of electrodes in it. During the charging of the metal-ion batteries, the electrolyte ions are stored in the pores of the active material used for the fabrication of electrodes in it [5–8]. Also, the specific capacity and energy density of the metal-ion batteries depend on the shape, size, porosity, and structure of the electrode material used in it. Many recent reports demonstrated that advanced synthesis techniques can easily control the shape, size, porosity, and structure of the electrode material. In consequence, the output parameters such as high energy density, high power density, and long cycle life of the battery can be controlled via tailoring the electrode material. Therefore, for enhancement of output parameters of batteries, and fabrication of high-performance electrodes for metal-ion batteries, for many years the researchers majorly focused on the development of advanced materials for anode and cathode for metal-ion batteries [8–10].

There are various active materials, such as layered and tunnel-type transition metal oxides, ternary metal oxides, transition metal hydroxides, transition metal fluorides, oxyanionic compounds, polymers, Prussian blue analogs, etc., on the other hand, graphitic and non-graphitic carbon materials are one of the most successful candidates as the anode for metal-ion batteries. In addition, tin-based material, silicon-based material, transition metal oxides, transition metal sulfides, and organic materials like Schiff bases, etc., have been used as the anode material for metal-ion batteries [3,6,11].

5.2 NANOCOMPOSITES FOR METAL-ION BATTERIES

In most of the MIBs, graphite has been used as an anode. The graphite is widely sourced and abundant in nature, and low cost. In addition, graphite shows excellent electrochemical performance with stable behavior in solid as well as liquid electrolytes. Also, the graphite anode in MIBs demonstrated equal theoretical and practical volumetric capacitance. However, MIBs containing graphite anode are unstable, which shows side reactions during the charging and discharging process. Also, an accommodation of metal ions is very difficult and is still a challenge for metal- (Na-, Al-, and Mg-) ion batteries containing graphite material as an anode. In the case of commercial graphite, the intercalation of metal ions into it is very difficult. As a consequence, metal-ion batteries with commercial graphite result in a very low volumetric capacity, energy density, and cycle life. Therefore, it is a very prime requirement to find a suitable anode material for metal- (Na-, Al-, and Mg-) ion batteries [10–12].

To date, there are many anode materials for MIBs. This includes carbon-based materials, metal oxide, metal sulfides, the nanocomposite of carbon-based materials with different metal oxides and metal sulfides, etc. The carbon-based nanocomposites are an efficient anode material for MIBs. The carbon metal oxides and carbon metal sulfide nanocomposites have been excessively used and demonstrated to be excellent anode materials for MIBs. The MIBs with carbon nanocomposites are reported to be high volumetric capacity, high energy density, and excellent cyclic stability [5,13]. Also, the synthesis of carbon-based nanocomposites is an easy and simple process. The existence of nanosized carbon in nanocomposites retains the high electrical conductivity, and high mechanical strength and has high structural stability in anode material. To date, the nanocomposites of nanostructured metal oxides and/or metal sulfides with different carbon nanostructured material viz. carbon nanotubes, single-walled carbon nanotubes, multiwalled carbon nanotubes, etc. have been heavily explored, and excessively used as the anode material for MIBs [5,9,11,14]. The latest development in the field of nanotechnology makes an easy synthesis of a variety of nanostructures, viz, nanotubes, nanowires, nanoneedles, nanobelts, etc. These attractive nanostructured materials have unique geometry with a high aspect ratio, due to that, these materials exhibit excellent physical and electrochemical properties [15–18].

5.3 TYPES OF MIBS AND THEIR WORKING PRINCIPLE

5.3.1 The Energy Storage Mechanism of LIBs

Using $LiCoO_2$ as a cathode material andgraphite (C) as the anode material, equations 5.1–5.3 demonstrate the energy storage mechanism of typical LIBs. During the charging of LIBs the lithium metal ions (Li^+) de-intercalate at the cathode material $LiCoO_2$. After de-intercalation Li^+ diffused into the electrolyte present between the cathode and anode in the LIB cell. Further, Li^+ passes through the nanopores and separates toward the graphite anode. Simultaneously, to maintain the charge neutrality through an external circuit the electrons move in the opposite direction. While during the discharging the Li^+ ion moves from an anode (C) to cathode $LiCoO_2$ [3,9]. The schematics of the charge-discharge mechanism of LIBs are demonstrated in **Figure 5.1**.

$$\text{Cathode: } LiCoO_2 \underset{\text{Discharge}}{\overset{\text{Charge}}{\rightleftharpoons}} Li_{(1-x)}CoO_2 + xLi^+ + xe^- \tag{5.1}$$

$$\text{Anode: } 6C + xLi^+ + xe^- \underset{\text{Discharge}}{\overset{\text{Charge}}{\rightleftharpoons}} Li_xC_6 \tag{5.2}$$

$$\text{Net reactions: } LiCoO_2 + 6C \underset{\text{Discharge}}{\overset{\text{Charge}}{\rightleftharpoons}} Li_{(1-x)}CoO_2 + Li_xC_6 \tag{5.3}$$

5.3.2 Charge Storage Mechanism in NIBs

In NIB_s the Na^+ can be inserted into the host of active materials at electrodes via three types of charge storage mechanisms viz. intercalation, alloying, and conversion. The intercalation can also be termed insertion. In the intercalation process, the Na^+ can be inserted into the host active material or the anode materials. The structural changes of the anode material have been retained in the intercalation process. The alloying mechanism can also be termed a solid-state reaction mechanism. In this mechanism, the Na^+ metal can beinserted into the host electrode material via reaction 5.4. Where A is the active material or metal electrode. In the alloying mechanism, the no phase transformation occurred [19]. The conversion mechanism is a relatively new mechanism that is still under development. The conversion mechanism results in a very high volumetric capacity of NIBs. In the

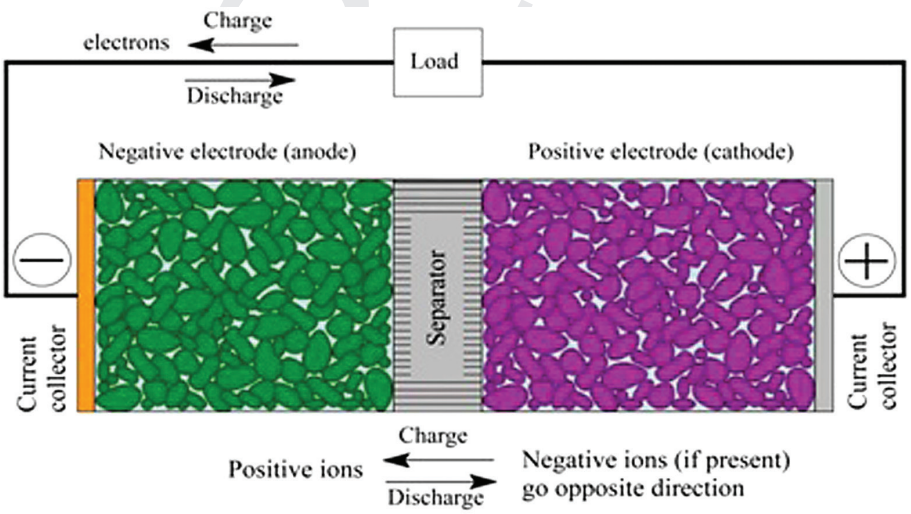

FIGURE 5.1 Schematics of the charge-discharge mechanism of LIBs. Adapted with permission. Copyright © 2020 by the authors. Licensee MDPI, Basel, Switzerland, distributed under the terms and conditions of the Creative Commons Attribution (CC BY) license (http://creativecommons.org/licenses/by/4.0/).

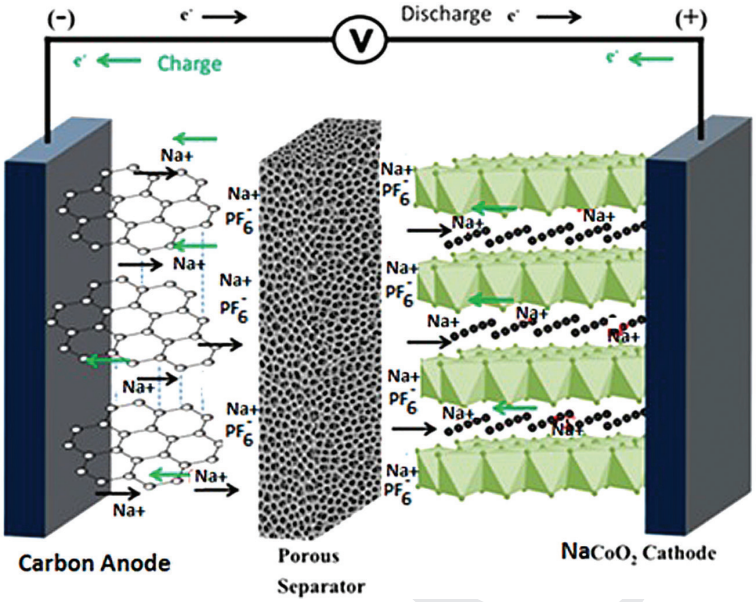

FIGURE 5.2 Schematics of charge–discharge mechanism of NIBs. Adapted with permission. Copyright (2020) American Chemical Society.

conversion mechanism, compared with the intercalation and alloying mechanism, the large volume expansion and heavy voltage hysteresis are persisted. These are the two major shortcomings of the conversion mechanism [20,21]. The schematics of the charge–discharge mechanism of NIBs are shown in **Figure 5.2**.

$$x\mathrm{Na}^{+} + \mathrm{A} + x\mathrm{e}^{-} \longleftrightarrow \mathrm{Na}_x\mathrm{A} \tag{5.4}$$

5.4 NWS IN MIBS

5.4.1 Nanowires in Lithium-Ion Batteries (LIBs)

The volume expansion, pulverization, and shifting effect are the major serious issues of MIBs. To avoid such problems, recently different strategies have been introduced in the literature. The application of different carbon composites with ternary metal sulfide and metal oxide is one of the important remedies. The nanostructure materials have a good aspect ratio, high mechanical strength, high surface area, large electrolyte electrode interface area, etc., such outstanding characteristics of nanostructured material reduce the charging-discharging time, provide the excellent electron transmission path decrease the electrode-electrolyte pathway to enhance the electrochemical activity of metal ion in MIBs [2,23,24]. To enhance the charge capacity, cycle life, and enhanced electrochemical characteristics of MIBs the different carbon structures such as nanostructure, nanorods, nanotubes, nanowire, nanobelt, and nanofiber are highly appreciated [8,17,18].

However, the synthesis of different carbon structures required complex reactions, multi-step processes, and high temperatures. Also, during synthesis, it is a very difficult task to control the carbon structure and maintain structural uniformity. Also, the low electrical conductivity and huge volume expansion of metal sulfides hinder its practical applications. Recently, the highly conductive and moderate ion size metal insertion in metal sulfide and metal oxide is one of the important remedies to these problems in MIBs. The application of metal-inserted metal sulfide nanowire electrodes is one of the important remedies to reduce cycle loss and improve the electrochemical

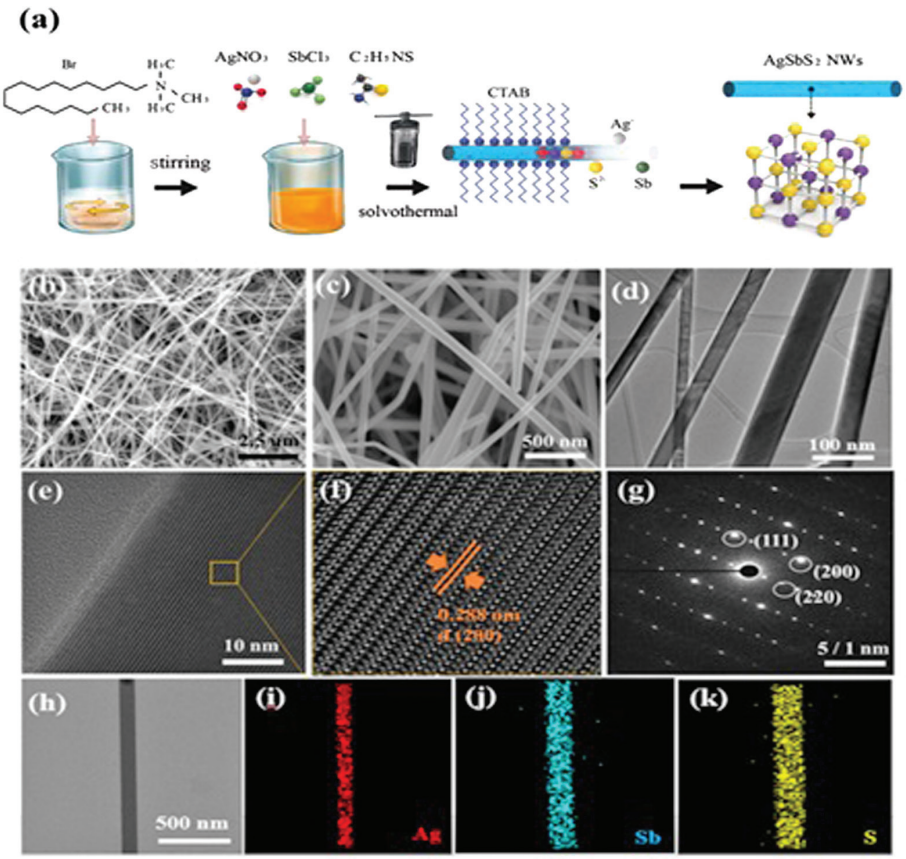

FIGURE 5.3 (a) Schematic demonstration of synthesis $AgSbS_2$ nanowires via hydrothermal method. (b, c) SEM images scanning electron microscope images (SEM), (d) Transmission electron microscope images, (e, f) High-resolution transmission electron microscope images, images, and (g) selected area diffraction pattern of $AgSbS_2$ nanowires. (h-k) energy dispersive X-ray spectroscopy mapping images of Ag, S, and Sb in $AgSbS_2$ nanowires. Adapted with permission. Copyright (2022) Elsevier.

behavior of metal sulfide and metal oxide-based MIBs [4,25,26]. To demonstrate this fact and for the enhancement of volumetric capacitance and cycle life of LIBs, Ho *et al.* [26] reported the insertion of silver-doped SbS_2 nanowires via the hydrothermal method as the anode material for LIBs. **Figure 5.3a** demonstrates the schematic of the synthesis $AgSbS_2$ nanowires via the hydrothermal synthesis route. A hydrothermal method is one of the simple and low-cost synthesis methods for uniform and hierarchical nanostructured materials [12,27,28]. Further, **Figures 5.3b-c** show the scanning electron microscope (SEM) images, demonstrating the morphology and average diameter (10–40 nm) of $AgSbS_2$ nanowires. **Figure 5.3d** shows transmission electron microscopy (TEM) images that depict the straight morphology of $AgSbS_2$ nanowires. The high-resolution transmission electron microscope (HRTEM) images (**Figures 5.3e-f**), and the selected area diffraction pattern (SAED) (**Figure 5.3g**) of $AgSbS_2$ nanowires demonstrated the single crystal of $AgSbS_2$ nanowires. Moreover, the uniform distribution of Ag, Sb, and S elements are conformed via energy dispersive X-ray spectroscopy mapping images and demonstrated in **Figures 5.3h-k**. In this report, the presence of Ag metal in SbS_2, enhances the electrical conductivity of the host material, reduced the volume change during cycling, constrains the shuttling effect of sulfur, and enhanced the lithium-ion absorption to improve the electrochemical performance of metal sulfide in LIBs. Using the $LiNi_5Co_3Mn_2$ cathode, $AgSbS_2$ anode and electrolyte 1 M $LiPF_6$, the full cell of LIBs demonstrated a

high discharge capacity of 904.5 mAh/g with an initial Coulombic efficiency of 62.3%. More interestingly, due to reaching a Coulombic efficiency of 99% per cycles and capacity retention of 90.6% over 7000 charge discharge cycle at 2A/g makes the $AgSbS_2$ anode material a super stable material for LIBs. Similarly, Lan *et al*. synthesized the silver-doped one-dimensional (1D) attapulgite (hydrated magnesium-aluminum rich silicate mineral) via in-situ reduction of silver nitrate onto the attapulgite as anode material LIBs The discharge specific capacity for silver-doped attapulgite anode-based LIBs is reported to be 133.0 mAh/g at a current density of 0.1 A/g after 50 cycles [29].

Guo *et al.* [30] reported the synthesis of ternary Fe_7S_8/SiO_x/nitrogen-doped carbon matrix by hydrothermal method and subsequent sulfur. The matrix has been utilized as an anode for LIBs. The presence of the reported matrix SiO_x/nitrogen-doped carbon in Fe_7S_8 enhances the electrical conductivity and provides improved electrical performance, cycle life, and reverse capacity of LIBs fabricated using Fe_7S_8/SiO_x/nitrogen-doped carbon as the anode with a charge capacity of 1060.2 mAh/g at 200 cycles along with an excellent cyclic performance of 415.8 mAh/g at the 1000th cycle at 5 A/g. Li *et al*. [31] reported the antimony sulfide (Sb_2S_3) nanowires on reduced graphene oxide composite synthesized by the self-assembly method. The as-reported three-dimensional (3D) architecture demonstrated an excellent electrochemical behavior as an anode in LIBs and effectively reduced volume change and improved the conductivity of Sb_2S_3. The morphology and structure of reduced graphene oxide (rGO), antimony sulfide (Sb_2S_3) nanowires and antimony sulfide (Sb_2S_3) nanowires reduced graphene oxide (rGO) composite are shown in **Figure 5.4a-f**. Further,

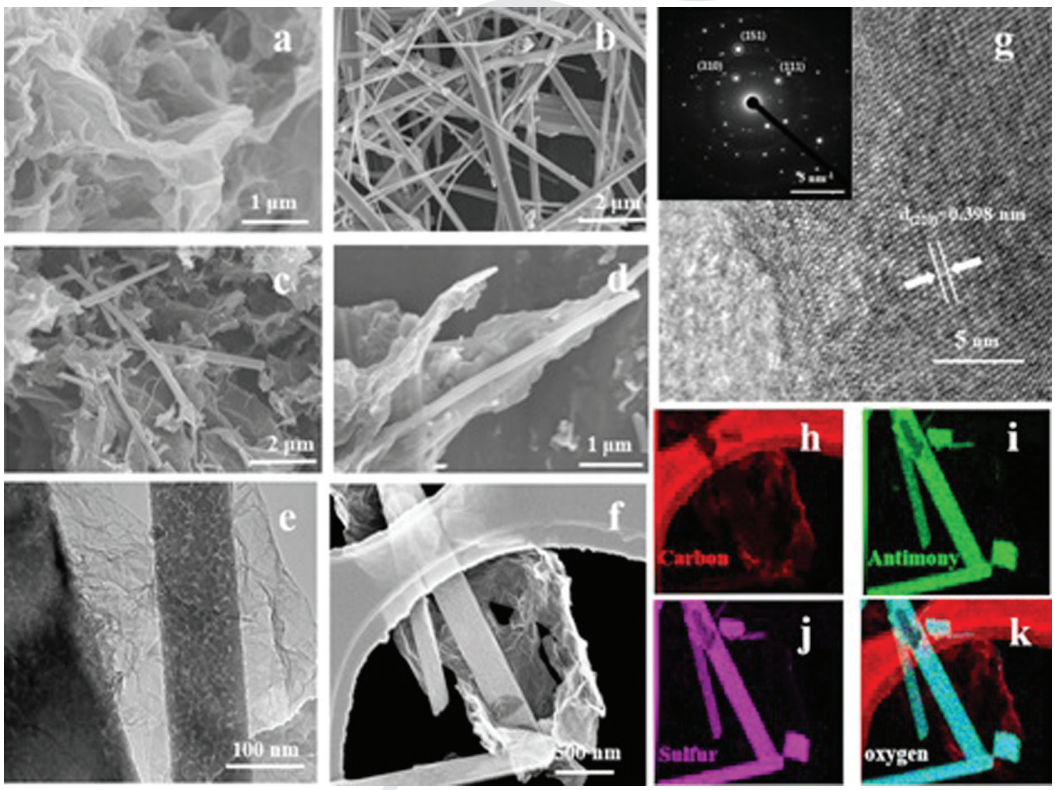

FIGURE 5.4 (a) Scanning electron microscopy (SEM) images of reduced graphene oxide (rGO), (b) SEM images of antimony sulfide (Sb_2S_3) nanowires, (c) low magnification, (d) high magnification SEM images of antimony sulfide (Sb_2S_3) nanowires, (e, f), high-resolution transmission electron microscopy (HRTEM) images, (g) corresponding SAED pattern (inset) of antimony sulfide (Sb_2S_3) nanowires reduced graphene oxide (rGO) composite, and (h), (i), (j), (k) elemental mapping of C, Sb, S, and O, respectively. Adapted with permission. Copyright (2021) Elsevier.

the elemental mapping of C, Sb, S, and O is confirmed via EDS elemental mapping (**Figure 5.4h-k**). The 3D architecture as the reported composite shows the reversible capacity of 505 mAh/g at 3 A/g and long cycle stability 697 mAh/g after 100 cycles at 100 mA/g. The electrochemical performance of the antimony sulfide (Sb_2S_3) nanowire reduced graphene oxide (rGO) composite is demonstrated in **Figure 5.5**. The antimony sulfide (Sb_2S_3) nanowire reduced graphene oxide (rGO) shows superior electrochemical performance over reduced graphene oxide (rGO) and antimony sulfide (Sb_2S_3)

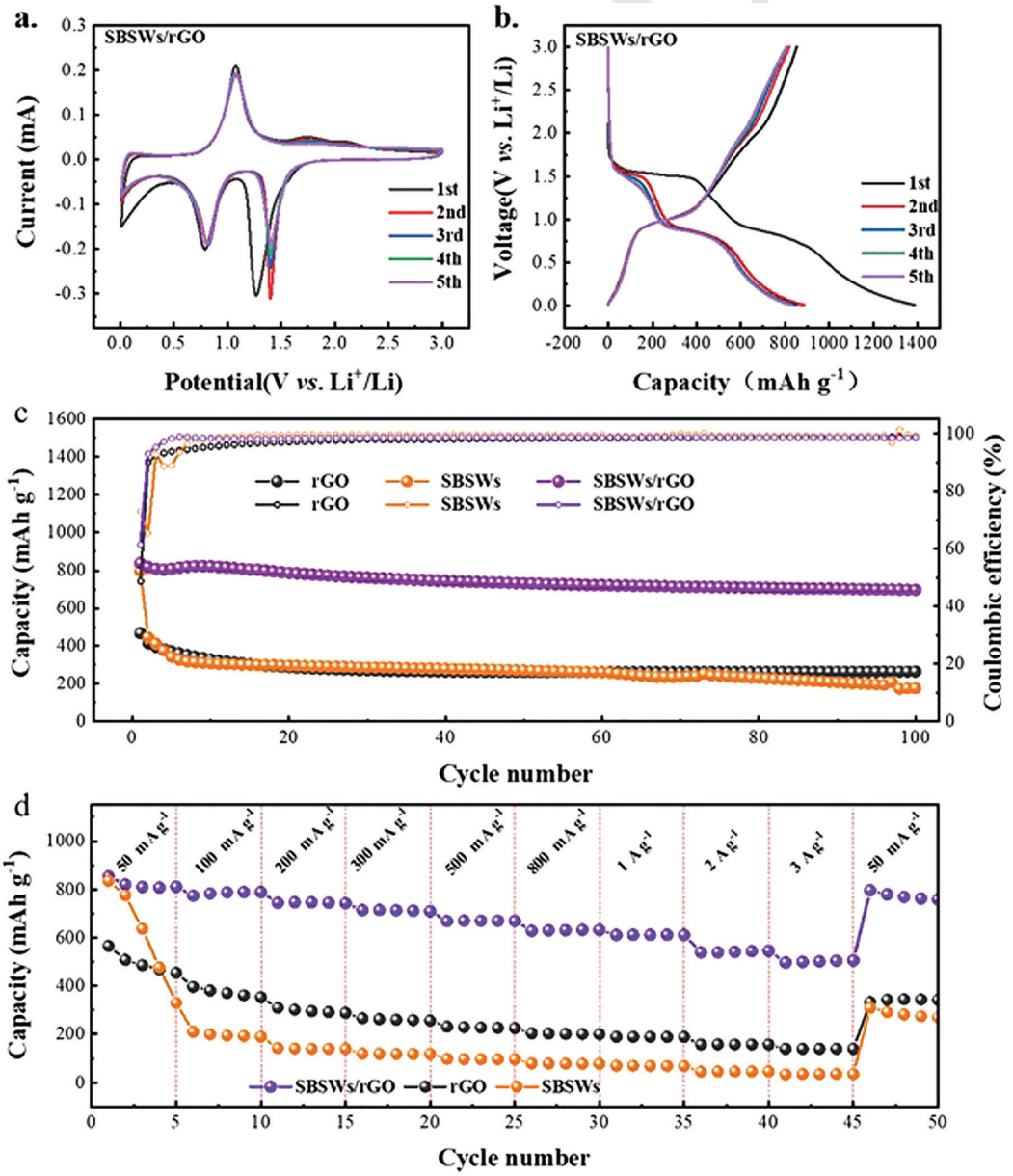

FIGURE 5.5 Cyclic voltammetry curves (0.01–3.00 V at 0.1 mV/s) (a), voltage profiles of antimony sulfide (Sb_2S_3) nanowire reduced graphene oxide (rGO) composite at 50 mA/g (b), cycle performances at 100 mA/g (c) and rate capability (d) for nanowires reduced graphene oxide (rGO) antimony sulfide (Sb_2S_3) nanowires and antimony sulfide (Sb_2S_3) nanowire reduced graphene oxide (rGO) composite electrodes. Adapted with permission. Copyright (2021) Elsevier.

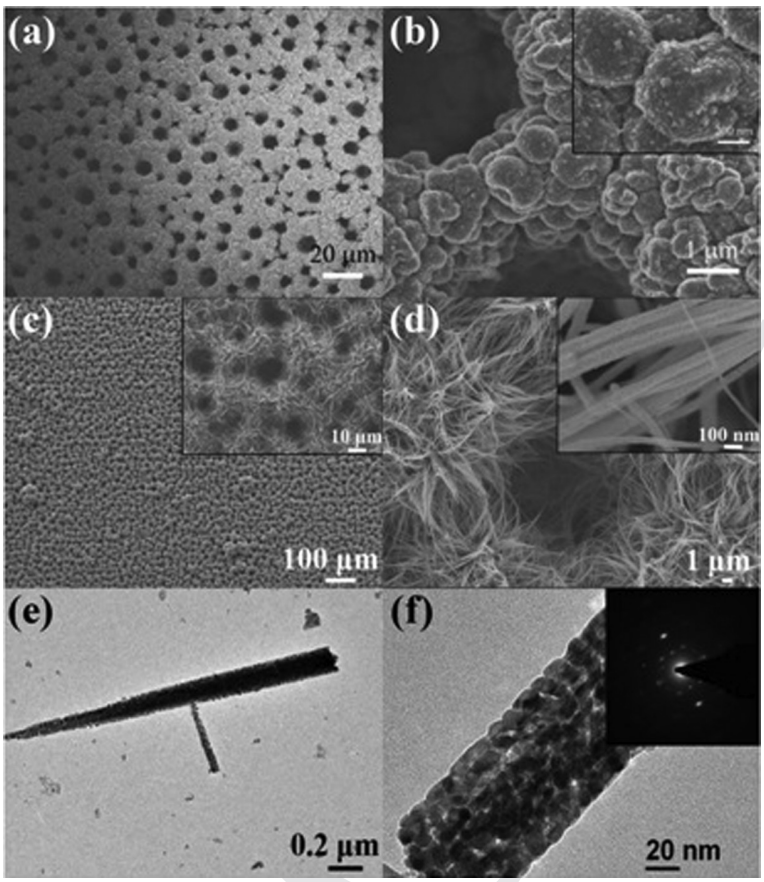

FIGURE 5.6 (a, b) Scanning electron microscopy images with low and high magnification of the Ni-Co_3O_4 dense film; (c, d) SEM images with low and high magnification of the Ni-Co_3O_4 nanowires; (e, f) transmission electron microscopy images with low and high magnification of the Ni-Co_3O_4 nanowires (selected area diffraction pattern (SAD) shown in inset). Adapted with permission. Copyright (2016) Elsevier.

nanowires. Moreover, the presence of reduced graphene oxide in antimony sulfide (Sb_2S_3) nanowires reduces the Li^+ diffusion path, can provide the space for shortening the Li^+ diffusion path, reduce the volume change, improve the electrical conductivity of the composite, and enhance the electron transfer between electrode-electrolyte interface and improve the rate performance.

Xiong *etal*. [32] prepared the 3D Ni-Co_3O_4 with nanowire porous branches and interconnected pore material by electrodeposition followed by the hydrothermal method. **Figure 5.6** shows the porous branches and interconnected pores of Ni-Co_3O_4 dense film Ni-Co_3O_4 nanowires. Compared with the dense Co_3O_4 film, the reported nanowire shows excellent electrochemical characterization. The Ni-Co_3O_4 with nanowire electrode demonstrates higher discharge capacities and high cycling stability of 714 mAh/g at 0.5 A/g after 100 cycles.

Usually, the binder used for the fabrication of electrodes introduces its resistivity into the electrode, which further influences the electrochemical activities of the anode in LIBs. Therefore, the fabrication of binder-free electrodes gains enormous attention. Many advanced strategies are used for the fabrication of thin films of active material electrodes. In this context, Wu *et al.* [33] synthesized the porous nanowire of porous NiO nanowires and coated it with Zr-based metal-organic gel (Zr-MOG), and used it as an electrode in LIBs. The LIBs with this electrode showed an excellent electrochemical performance with a specific capacity of 1816.3 mAh/g at a current density of 100 mA/g,

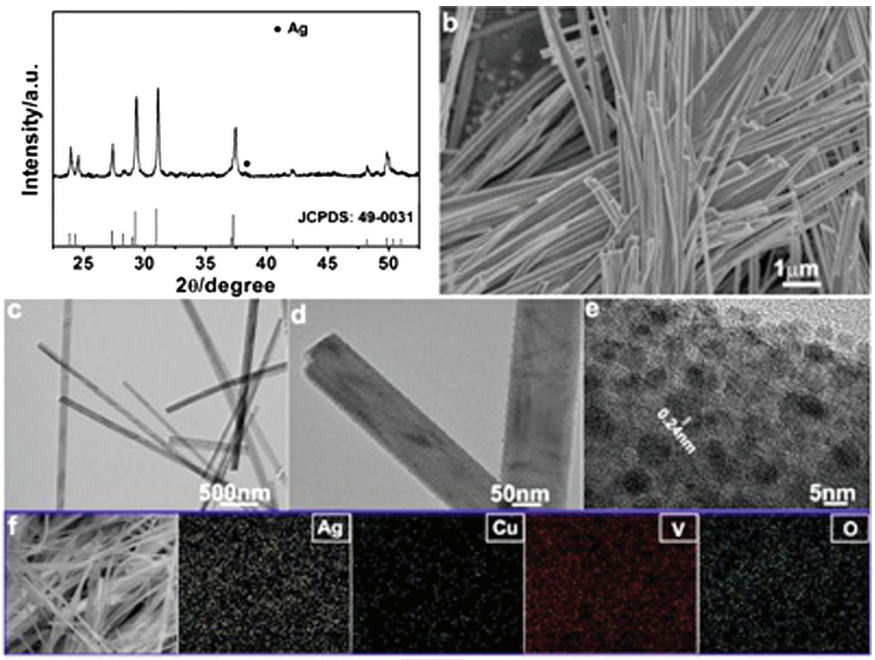

FIGURE 5.7 $Ag_2Cu(VO_3)_4$/Ag nanowires (a) XRD pattern, (b) FESEM, (c–e) TEM and (f) SEM-EDX mapping images. Adapted with permission. Copyright (2021), Elsevier.

and capacitance retention of 1318.7 mAh/g over 150 charge-discharge cycles. Similarly, Zhang *et al.* synthesized quaternary transition-metal vanadium oxide $Ag_2Cu(VO_3)_4$/Ag nanowires (**Figure 5.7**) by a simple hydrothermal method used as the cathode material for LIBs. Electrochemical measurement shows that the $Ag_2Cu(VO_3)_4$/Ag nanowires are a new cathode material with good electrochemical performance and the discharge capacity can be stabilized at 132.4 mAh/g after 50 cycles at 200 mA/g. Moreover, the recent advancement in the nanostructured material used as an electrode for LIBs is illustrated in **Table 5.1**.

5.4.2 Nanowires in Sodium-Ion Batteries (SIBs)

Sodium ion batteries (SIBs) are another promising energy storage system in comparison to LIBs. SIBs have low cost and equivalent electrochemical principle to LIBs. However, major issues like a large radius of Na^+ (1.02 Å) than Li^+ vs. Li^+ (0.76 Å), lower electrochemical activity than LIBs, and serious safety issues (fire or explosion due to the high flammability of organic solvents), etc., need more research and development in electrodes and electrolytes used in NIBs. Therefore, to make the availability of user-friendly NIBs to fulfill global energy needs, the development of NIBs is searching for suitable anode, cathode, electrode, binder, and separator materials to improve their electrochemical performance [48,49].

To tackle the issues and remove the existing problems of the NIBs, recently many recent reports suggested solutions and reported advanced strategies. The use of nanostructure single/binary/ternary metal sulfide, metal oxide, and their composites with different carbon materials as an electrode is one of the important remedies to the problem associated with NIBs. For example, Cao *et al*. [50] reported the single crystalline $Na_4Mn_9O_{18}$ nanowires synthesized by template-assisted sol-gel method. The reported electrode material shows high crystallinity, pure phase, and homogeneous size, using the $Na_4Mn_9O_{18}$ nanowires as the cathode, the as-fabricated NIBs show excellent

TABLE 5.1
Recent Advancement in the Nanostructured Material used as an Electrode for LIBs

Sr. No.	Materials	Method of synthesis	Operating voltage	Electrolyte	Specific capacitance	Retention of capacity	Reference
1.	Li_2MnO_3	Molten-Salt method.	2.0–4.8 V.	Dimethyl carbonate (DMC)	194.4 mAh/g	88.2% after 20 cycles at 0.1C	[34]
2.	Si/Cu	The pulsed electrical discharge method and chemical etching.	0.01–2 V	$LiPF_6$ 1 mol/L	1456 mAh/g	86.5% after 500 cycles.	[35]
3.	$CeVO_4$-V_2O_5	Cation-exchange and heat-treatment route	0.01–3 V	1 M $LiPF_6$	487 mAh/g		[36]
4.	Cu/Cu_2O@ Ppy	One-step hydrothermal method	0.01–3.0 V.	$LiPF_6$ in EC + DMC1 mol/L	787 mAh/g		[37]
5.	SiC	Electro-deoxidation	0–3.0 V	1 M $LiPF_6$	1000 mAh/g	99% over hundreds of cycles.	[38]
6.	GeSe	Rapid thermal processing method	0.01–3.0 V	1 M $LiPF_6$	~815.49mAh/g		[39]
7.	MnO/Sb@NC	Hydrothermal-mixing-Calcination	0.01–3.0 V	1.0 M $LiPF_6$	664 mAh/g	89.15% after 1100 cycles	[40]
8.	$ZnFe_2O_4$@ polypyrrolE	Electrospinning technique with gas-phase polymerization	0.01–3.0 V	1 M $LiPF_6$	~881 mAh/g		[41]
9.	GaZnON	Chemical vapor deposition	0.01–3.0 V	1 M $LiPF_6$	878.2 mAh/g		[42]
10.	AgNWs@Si@GO	Thermal reduction, Hummers' method	0–3.0 V	1 M $LiPF_6$	830 mAh/g	94% after 70 cycles	[43]
11.	$MnMoO_4$/C	Top-down tailoring strategy	0.01–3.0 V.	1M $LiPF_6$	994 mAh/g	90% after 100 cycles	[44]
12.	CeB_6	Low-temperature solution combustion method	0.01–3.0 V	1M $LiPF_6$	200 mAh/g	~99% . After the 80 or 100 cycles	[45]
13.	Fe_3O_4	A facile deposition immersion calcination process	0.05–3.0 V.	1M $LiPF_6$	100 mAh/g	93.6% after100 cycles	[46]
14.	TiO_2	Simple hydrothermal reaction	2.6–0.8 V a	1 mol L^{-1} $LiPF_6$ and ethylene carbonate (EC)/dimethyl carbonate	280 mAh/g	~98% after 40 cycles	[47]

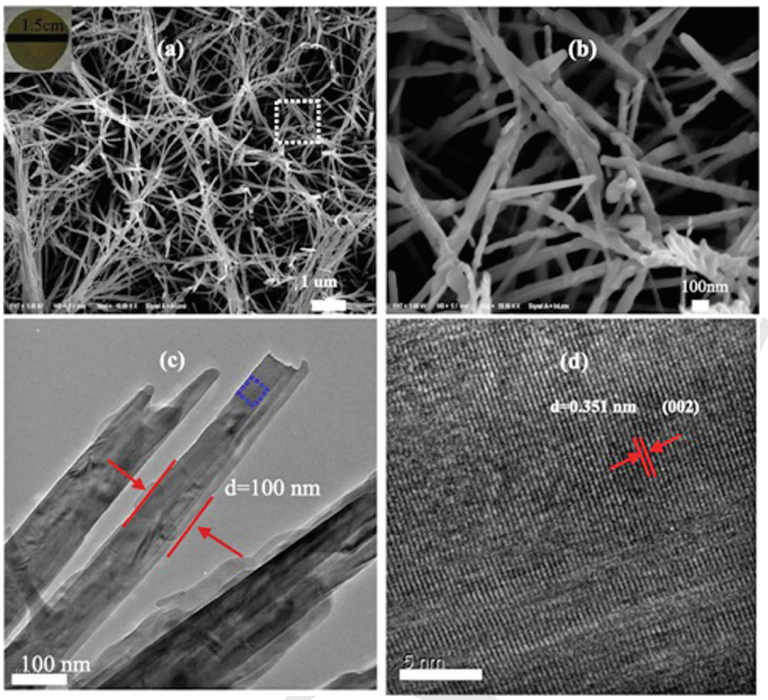

FIGURE 5.8 (a) SEM images of the samples on Ti foil annealed at 250 °C, inset in (a) is a digital photo of the entire sample; (b) high-resolution SEM image from the marked in area (a); (c) TEM image of several nanowires; (d) HR-TEM image of a $Na_5V_{12}O_{32}$ nanowire. Adapted with permission. Copyright (2019) Elsevier.

electrochemical performance, high capacity of 109 mAh/g at 0.5C, and capacity retention of 77% of this value even after 1000 charge/discharge at 0.5 C. Similarly, Ta *et al.*reported the synthesis of $Na_4Mn_9O_{18}$ nanowires via simple and low-cost hydrothermal method [51]. Using $Na_4Mn_9O_{18}$ nanowires as a cathode in NIBs demonstrated excellent electrochemical performance, delivering a high capacity of 90 mAh/gand Coulombic efficiencies of greater than 91% at a rate of 0.2C during 30 charge/discharge. Interestingly, Cao *et al.* [52] reported the first time use of the sodium vanadate ($Na_5V_{12}O_{32}$) array nanowire (**Figure 5.8**) on titanium foil synthesis via the hydrothermal synthesis route. The electrochemical performance of sodium vanadate nanowires is illustrated in **Figure 5.9**. The sodium vanadate nanowires demonstrated excellent electrochemical performance and resulted in 166 and 161 mAh/g charge/discharge capacities at a current density of 30 mA/g, respectively, and retained a capacity of 130 mAh/g after 40 cycles. Moreover, the recent advancement in the nanostructured material used as an electrode for NIBs is illustrated in **Table 5.2**.

5.5 CONCLUSIONS

In conclusion, the recent advancements in designing and fabrication of NW electrodes for MIBs have been summarized. The electrode materials for MIBs countenance various factors viz. material properties and volume, etc. Providentially, the NWs have given rise to MIBs with improved performance. The unique structural feature of the NWs offers their high performance. Compared to conventional electrodes, NW electrodes tender various advantages as electrodes for MIBs, which includes the following: (i) compliant volume changes during the metal-ion insertion/extraction; (ii) simple ion diffusion mechanism; (iii) effective charge transfer; (iv) tough structural permanence.

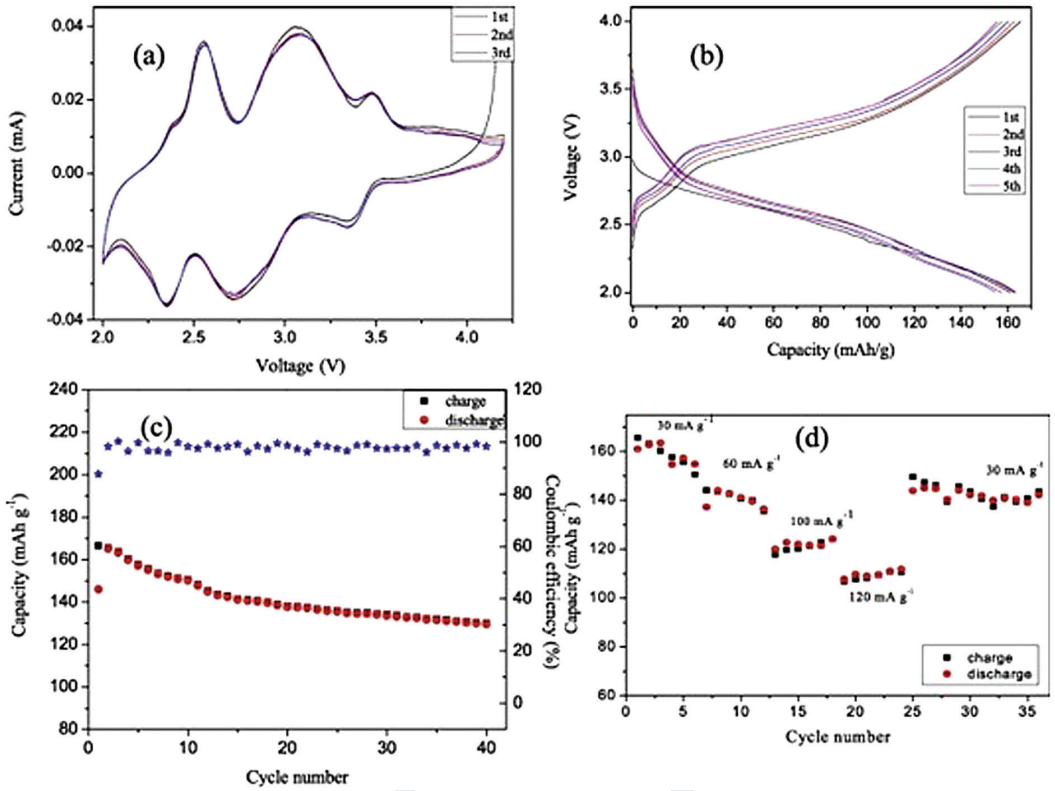

FIGURE 5.9 (a) Cyclic voltammograms of $Na_5V_{12}O_{32}$ nanowire arrays at a scan rate of 0.5 mV/s between 2.0 and 4.0 V; (b) the first five galvanostatic charge/discharge cycles at a current density of 30 mA/g; (c) capacity retention of the galvanostatic test at a current density of 30 mA/g; (d) charge-discharge capacities at various current densities of 30–120 mAh/g. Adapted with permission. Copyright (2019) Elsevier.

TABLE 5.2
Recent Advancements in the Nanostructured Material used as an Electrode for NIBs.

Sr. No.	Material	Method of synthesis	Electrolyte	Operating voltage	Capacitance	Coulombic efficiencies	Reference
1	TiO_2-x/Sb	Chemical de-alloying method	0.1 to 2.0 V	1 M $NaClO_4$	591.9 mAh/g	96.4% after 200 cycles	
2	MnO_2@rGO	Mno_2@rgo	0.01 to 3.0 V	1 M $NaClO_4$	250 mAh/g	81.7% over 400 cycles	[53]
3	hydrogen titanate	Alkali hydrothermal Process, thermal reduction	0.0 to 2.5 V	1.0 M $NaClO_4$ PC/EC	238 mAh/g	80.6% after 4200 cycles	[54]
4	$Na_3V_2(PO_4)_3$/C.	Agar-gel combined freeze-drying method	1.0 to 2.5 V	0.8 M $NaPF_6$/EMC + PC + FEC	113.4 mAh/g	88.2% after 1000 cycles	[55]
5	VS_4@L-Ti_3C_2Tx	Hydrothermal	0.01–4.0 V	1 M $LiPF_6$	599 mAh/g	67% after 6700 cycles	[56]
6	Fe_3O_4@C/rGO	In-situ plantation	1.0 M $LiPF_6$	0.01–3.0 V	429 mAh/g		[57]
7	WS_2/hollow carbon composite	Hydrothermal	1 M $NaPF_6$	0.01–3 V.	575 mAh/g	76.6%after 80 cycles	[58]
8	MWCNT@ polyimide	Thermal imidization	1.0 M Na_2SO_4	-1.0–0.0 V	209.3 mAh/g	77.8%. after 100 cycles	[59]
9	MnO_2@rG	Hydrothermal method	1 M KPF_6	0.01–3 V	389 F/g	81.7% over 500 cycles	[60]
10	VO_2 (A)/graphene nanostructure	Hydrothermal	1.0 M $NaClO_4$	1–4 V	——	115 mAh/g over 100 cycles at a current density of 100 mA/g.	[61]

REFERENCES

[1] N. Singh, K. Banerjee, M. Gupta, Y.K. Bainsla, V.U. Pandit, P. Singh, S.J. Uke, A. Kumar, S.P. Mardikar, Y. Kumar, Concentration dependent electrochemical performance of aqueous choline chloride electrolyte, Mater. Today Proc. 53 (2022) 161–167.

[2] X. Cao, X. Ren, L. Zou, M.H. Engelhard, W. Huang, H. Wang, B.E. Matthews, H. Lee, C. Niu, B.W. Arey, Monolithic solid–electrolyte interphases formed in fluorinated orthoformate-based electrolytes minimize Li depletion and pulverization, Nat. Energy. 4 (2019) 796–805.

[3] J. Verma, D. Kumar, Metal-ion batteries for electric vehicles: current state of the technology, issues and future perspectives, Nanoscale Adv. 3 (2021) 3384–3394.

[4] Z. Pang, B. Ding, J. Wang, Y. Wang, L. Xu, L. Zhou, X. Jiang, X. Yan, J.P. Hill, L. Yu, Metal-ion inserted vanadium oxide nanoribbons as high-performance cathodes for aqueous zinc-ion batteries, Chem. Eng. J. 446 (2022) 136861.

[5] C. Shi, K.A. Owusu, X. Xu, T. Zhu, G. Zhang, W. Yang, L. Mai, 1D carbon-based nanocomposites for electrochemical energy storage, Small. 15 (2019) 1902348.

[6] M. Mallik, M. Saha, Carbon-based nanocomposites: Processing, electronic properties and applications, in: Carbon Nanomater. Electron. Devices Appl., Springer, 2021: pp. 97–122.

[7] D. Majumdar, M. Mandal, S.K. Bhattacharya, V_2O_5 and its carbon-based nanocomposites for supercapacitor applications, ChemElectroChem. 6 (2019) 1623–1648.

[8] R. Febrian, N.L.W. Septiani, M. Iqbal, B. Yuliarto, Recent advances of carbon-based nanocomposites as the anode materials for lithium-ion batteries: Synthesis and performance, J. Electrochem. Soc. 168 (2021) 110520.

[9] Y. Chen, Y. Kang, Y. Zhao, L. Wang, J. Liu, Y. Li, Z. Liang, X. He, X. Li, N. Tavajohi, A review of lithium-ion battery safety concerns: The issues, strategies, and testing standards, J. Energy Chem. 59 (2021) 83–99.

[10] N. Singh, K. Banerjee, Y.K. Bainsla, M.K. Singh, M. Gupta, A. Kumar, P. Singh, S.J. Uke, S.P. Mardikar, V.U. Pandit, Preparation of electrochemically stable choline chloride-sugar based sustainable electrolytes and study of effect of water on their electrochemical behaviour, Mater. Today Proc. 53 (2022) 179–184.

[11] S.J. Uke, S.P. Mardikar, A. Kumar, Y. Kumar, M. Gupta, Y. Kumar, A review of π-conjugated polymer-based nanocomposites for metal-ion batteries and supercapacitors, R. Soc. Open Sci. 8 (2021) 210567.

[12] S.J. Uke, D.S. Thakre, V.P. Akhare, G.N. Chaudhari, S.P. Meshram, PEG-600 assisted hydrothermal synthesis of $NiCo_2O_4$ as an electrode material for supercapacitor application, in: Proc. Int. Meet. Energy Storage Devices Ind.-Acad. Conclave, 2018.

[13] R. Sanjinés, M.D. Abad, C. Vâju, R. Smajda, M. Mionić, A. Magrez, Electrical properties and applications of carbon based nanocomposite materials: An overview, Surf. Coat. Technol. 206 (2011) 727–733.

[14] Y. Zhao, L.P. Wang, M.T. Sougrati, Z. Feng, Y. Leconte, A. Fisher, M. Srinivasan, Z. Xu, A review on design strategies for carbon based metal oxides and sulfides nanocomposites for high performance Li and Na ion battery anodes, Adv. Energy Mater. 7 (2017) 1601424.

[15] M. Li, J. Lu, K. Amine, Nanotechnology for sulfur cathodes, ACS Nano. 15 (2021) 8087–8094.

[16] P. Chen, C. Zhang, B. Jie, H. Zhang, K. Zhang, Y. Song, Large-scale preparation of cobalt niobate/reduced graphene oxide composite materials for high-performance lithium-ion battery anodes, J. Alloys Compd. 908 (2022) 164542.

[17] K. Yu, X. Pan, G. Zhang, X. Liao, X. Zhou, M. Yan, L. Xu, L. Mai, Nanowires in energy storage devices: Structures, synthesis, and applications, Adv. Energy Mater. 8 (2018) 1802369.

[18] G. Zhou, L. Xu, G. Hu, L. Mai, Y. Cui, Nanowires for electrochemical energy storage, Chem. Rev. 119 (2019) 11042–11109.

[19] Mostafa Al-Gabalawy, Nesreen S. Hosny, Shimaa A. Hussien. Lithium-ion battery modeling including degradation based on single-particle approximations, Batteries 2020, 6 (3), 37.

[20] Z. Wang, X. Yan, F. Wang, T. Xiong, M.-S. Balogun, H. Zhou, J. Deng, Reduced graphene oxide thin layer induced lattice distortion in high crystalline MnO_2 nanowires for high-performance sodium- and potassium-ion batteries and capacitors, Carbon. 174 (2021) 556–566.

[21] L. Gao, D. Lu, Y. Yang, R. Guan, D. Zhang, C. Sun, S. Liu, X. Bian, Amorphous TiO_{2-x} modified Sb nanowires as a high-performance sodium-ion battery anode, J. Non-Cryst. Solids. 581 (2022) 121396.
[22] K.M. Abraham, How comparable are sodium-ion batteries to lithium-ion counterparts? ACS Energy Lett. 5 (2020) 3544–3547.
[23] M. Ma, S. Zhang, L. Wang, Y. Yao, R. Shao, L. Shen, L. Yu, J. Dai, Y. Jiang, X. Cheng, Harnessing the volume expansion of MoS_3 anode by structure engineering to achieve high performance beyond lithium-based rechargeable batteries, Adv. Mater. 33 (2021) 2106232.
[24] W. An, B. Gao, S. Mei, B. Xiang, J. Fu, L. Wang, Q. Zhang, P.K. Chu, K. Huo, Scalable synthesis of ant-nest-like bulk porous silicon for high-performance lithium-ion battery anodes, Nat. Commun. 10 (2019) 1–11.
[25] H.-Y. Wang, H.-Y. Chen, Y.-Y. Hsu, U. Stimming, H.M. Chen, B. Liu, Modulation of crystal surface and lattice by doping: achieving ultrafast metal-ion insertion in anatase TiO_2, ACS Appl. Mater. Interfaces. 8 (2016) 29186–29193.
[26] S.-F. Ho, Y.-C. Yang, H.-Y. Tuan, Silver boosts ultra-long cycle life for metal sulfide lithium-ion battery anodes: Taking $AgSbS_2$ nanowires as an example, J. Colloid Interface Sci. 621 (2022) 416–430.
[27] S.J. Uke, G.N. Chaudhari, A.B. Bodade, S.P. Mardikar, Morphology dependant electrochemical performance of hydrothermally synthesized NiCo2O4 nanomorphs, Mater. Sci. Energy Technol. 3 (2020) 289–298.
[28] S.J. Uke, G.N. Chaudhari, Y. Kumar, S.P. Mardikar, Tri-ethanolamine-ethoxylate assisted hydrothermal synthesis of nanostructured $MnCo_2O_4$ with superior electrochemical performance for high energy density supercapacitor application, Mater. Today Proc. 43 (2021) 2792–2799.
[29] Y. Lan, D. Chen, Fabrication of silver doped attapulgite aerogels as anode material for lithium ion batteries, J. Mater. Sci. Mater. Electron. 29 (2018) 19873–19879.
[30] X. Guo, S. Wang, B. Yang, Y. Xu, Y. Liu, H. Pang, Porous pyrrhotite Fe7S8 nanowire/SiO_x/nitrogen-doped carbon matrix for high-performance Li-ion-battery anodes, J. Colloid Interface Sci. 561 (2020) 801–807.
[31] Z. Li, H. Du, J. Lu, L. Wu, L. He, H. Liu, Self-assembly of antimony sulfide nanowires on three-dimensional reduced GO with superior electrochemical lithium storage performances, Chem. Phys. Lett. 771 (2021) 138529.
[32] Q.Q. Xiong, H.Y. Qin, H.Z. Chi, Z.G. Ji, Synthesis of porous nickel networks supported metal oxide nanowire arrays as binder-free anode for lithium-ion batteries, J. Alloys Compd. 685 (2016) 15–21.
[33] D. Wu, L. Zhang, J. Zhang, Z. Zhang, F. Liang, L. Jiang, B. Tang, Y. Rui, F. Liu, Novel self-supporting multilevel-3D porous NiO nanowires with metal-organic gel coating via "like dissolves like" to trigger high-performance binder-free lithium-ion batteries, Microporous Mesoporous Mater. 328 (2021) 111483.
[34] Y. Sun, M. Guo, S. Shu, D. Ding, C. Wang, Y. Zhang, J. Yan, Preparation of Li2MnO_3 nanowires with structural defects as high rate and high capacity cathodes for lithium-ion batteries, Appl. Surf. Sci. 585 (2022) 152605.
[35] J. Hong, K. Cheng, G. Xu, M. Stapelberg, Y. Kuai, P. Sun, S. Qu, Z. Zhang, Q. Geng, Z. Wu, M. Zhu, P.V. Braun, Novel silicon/copper nanowires as high-performance anodes for lithium ion batteries, J. Alloys Compd. 875 (2021) 159927.
[36] X. Xu, S. Chang, T. Zeng, Y. Luo, D. Fang, M. Xie, J. Yi, Synthesis of $CeVO_4$-V_2O_5 nanowires by cation-exchange method for high-performance lithium-ion battery electrode, J. Alloys Compd. 887 (2021) 161237.
[37] Y. Wang, L. Cao, J. Li, L. Kou, J. Huang, Y. Feng, S. Chen, Cu/Cu2O@Ppy nanowires as a long-life and high-capacity anode for lithium ion battery, Chem. Eng. J. 391 (2020) 123597.
[38] D. Sri Maha Vishnu, J. Sure, H.-K. Kim, R.V. Kumar, C. Schwandt, Solid state electrochemically synthesised β-SiC nanowires as the anode material in lithium ion batteries, Energy Storage Mater. 26 (2020) 234–241.
[39] K. Wang, M. Liu, D. Huang, L. Li, K. Feng, L. Zhao, J. Li, F. Jiang, Rapid thermal deposited GeSe nanowires as a promising anode material for lithium-ion and sodium-ion batteries, J. Colloid Interface Sci. 571 (2020) 387–397.

[40] B. Wang, Y. Xia, Z. Deng, Y. Zhang, H. Wu, Three-dimensional cross-linked MnO/Sb hybrid nanowires co-embedded nitrogen-doped carbon tubes as high-performance anode materials for lithium-ion batteries, J. Alloys Compd. 835 (2020) 155239.
[41] L. Hou, R. Bao, D. kionga Denis, X. Sun, J. Zhang, F. uz Zaman, C. Yuan, Synthesis of ultralong $ZnFe_2O_4$@polypyrrole nanowires with enhanced electrochemical Li-storage behaviors for lithium-ion batteries, Electrochimica Acta. 306 (2019) 198–208.
[42] Y. Han, C. Sun, K. Gao, S. Ding, Z. Miao, J. Zhao, Z. Yang, P. Wu, J. Huang, Z. Li, A. Meng, L. Zhang, P. Chen, Heterovalent oxynitride GaZnON nanowire as novel flexible anode for lithium-ion storage, Electrochimica Acta. 408 (2022) 139931.
[43] J. Wei, C. Qin, X. Pang, H. Zhang, X. Li, One-dimensional core-shell composite of AgNWs@Si@GO for high-specific capacity and high-safety anode materials of lithium-ion batteries, Ceram. Int. 47 (2021) 4937–4943.
[44] L. Zhang, J. Bai, F. Gao, S. Li, Y. Liu, S. Guo, Tailoring of hierarchical $MnMoO_4$/C nanocauliflowers for high-performance lithium/sodium ion half/full batteries, J. Alloys Compd. 906 (2022) 164394.
[45] Z. Wang, W. Han, Q. Kuang, Q. Fan, Y. Zhao, Low-temperature synthesis of CeB6 nanowires and nanoparticles as feasible lithium-ion anode materials, Adv. Powder Technol. 31 (2020) 595–603.
[46] K. Cheng, F. Yang, K. Ye, Y. Zhang, X. Jiang, J. Yin, G. Wang, D. Cao, Highly porous Fe_3O_4–Fe nanowires grown on C/TiC nanofiber arrays as the high performance anode of lithium-ion batteries, J. Power Sources. 258 (2014) 260–265.
[47] Y. Wang, M. Wu, W.F. Zhang, Preparation and electrochemical characterization of TiO_2 nanowires as an electrode material for lithium-ion batteries, Electrochimica Acta. 53 (2008) 7863–7868.
[48] X. Chen, Y. Zhang, The main problems and solutions in practical application of anode materials for sodium ion batteries and the latest research progress, Int. J. Energy Res. 45 (2021) 9753–9779.
[49] M. Chen, Q. Liu, S.-W. Wang, E. Wang, X. Guo, S.-L. Chou, High-abundance and low-cost metal-based cathode materials for sodium-ion batteries: Problems, progress, and key technologies, Adv. Energy Mater. 9 (2019) 1803609.
[50] Y. Cao, L. Xiao, W. Wang, D. Choi, Z. Nie, J. Yu, L.V. Saraf, Z. Yang, J. Liu, Reversible sodium ion insertion in single crystalline manganese oxide nanowires with long cycle life, Adv. Mater. 23 (2011) 3155–3160.
[51] A.T. Ta, T.T.O. Nguyen, H.C. Le, D.T. Le, T.C. Dang, M.T. Man, S.H. Nguyen, D.L. Pham, Hydrothermal synthesis of $Na_4Mn_9O_{18}$ nanowires for sodium ion batteries, Ceram. Int. 45 (2019) 17023–17028.
[52] Y. Cao, J. Wang, X. Chen, B. Shi, T. Chen, D. Fang, Z. Luo, Nanostructured sodium vanadate arrays as an advanced cathode material in high-performance sodium-ion batteries, Mater. Lett. 237 (2019) 122–125.
[53] Z. Wang, X. Yan, F. Wang, T. Xiong, M.-S. Balogun, H. Zhou, J. Deng, Reduced graphene oxide thin layer induced lattice distortion in high crystalline MnO_2 nanowires for high-performance sodium- and potassium-ion batteries and capacitors, Carbon. 174 (2021) 556–566.
[54] M.-Y. Sun, F.-D. Yu, Y. Xia, L. Deng, Y.-S. Jiang, L.-F. Que, L. Zhao, Z.-B. Wang, Trigger Na+-solvent co-intercalation to achieve high-performance sodium-ion batteries at subzero temperature, Chem. Eng. J. 430 (2022) 132750.
[55] G. Cui, H. Wang, F. Yu, H. Che, X. Liao, L. Li, W. Yang, Z. Ma, Scalable synthesis of $Na_3V_2(PO_4)_3$/C with high safety and ultrahigh-rate performance for sodium-ion batteries, Chin. J. Chem. Eng. (2021).
[56] H. Wang, P. Wang, W. Gan, L. Ci, D. Li, Q. Yuan, VS_4 nanoarrays pillared $Ti_3C_2T_x$ with enlarged interlayer spacing as anode for advanced lithium/sodium ion battery and hybrid capacitor, J. Power Sources. 534 (2022) 231412.
[57] J.-L. Xu, X. Zhang, Y.-X. Miao, M.-X. Wen, W.-J. Yan, P. Lu, Z.-R. Wang, Q. Sun, In-situ plantation of Fe_3O_4@C nanoparticles on reduced graphene oxide nanosheet as high-performance anode for lithium/sodium-ion batteries, Appl. Surf. Sci. 546 (2021) 149163.
[58] W. Liu, M. Wei, L. Ji, Y. Zhang, Y. Song, J. Liao, L. Zhang, Hollow carbon sphere based WS_2 anode for high performance lithium and sodium ion batteries, Chem. Phys. Lett. 741 (2020) 137061.
[59] B. Cho, H. Lim, H.-N. Lee, Y.M. Park, H. Kim, H.-J. Kim, High-capacity and cycling-stable polypyrrole-coated MWCNT@polyimide core-shell nanowire anode for aqueous rechargeable sodium-ion battery, Surf. Coat. Technol. 407 (2021) 126797.

[60] Z. Wang, X. Yan, F. Wang, T. Xiong, M.-S. Balogun, H. Zhou, J. Deng, Reduced graphene oxide thin layer induced lattice distortion in high crystalline MnO_2 nanowires for high-performance sodium- and potassium-ion batteries and capacitors, Carbon. 174 (2021) 556–566.

[61] X. Hu, Z. Zhao, L. Wang, J. Li, C. Wang, Y. Zhao, H. Jin, VO_2 (A)/graphene nanostructure: Stand up to Na ion intercalation/deintercalation for enhanced electrochemical performance as a Na-ion battery cathode, Electrochimica Acta. 293 (2019) 97–104.

[62] Shaoyan Zhanga, Lijie Ci, Wei Mu, Hydrothermal synthesis of $Ag_2Cu(VO_3)_4$/Ag nanowires: A new cathode material for lithium-ion batteries, Scripta Materialia, 210, 2022, 114431